

Improving frequency domain deconvolution at low frequencies

Sina Esmaili and Gary F. Margrave

ABSTRACT

Finding the method to obtain the best reflectivity is always challenging. The accuracy of estimated reflectivity directly depends on how precise embedded wavelet is estimated. The frequency domain deconvolution algorithm, which is one of the deconvolution methods, estimates the reflectivity function via extracting wavelet from seismic data in frequency domain. This algorithm estimates the wavelet by smoothing the amplitude spectrum of the data. Therefore, the nature of the smoothing process in the deconvolution algorithm can affect the resulted reflectivity.

The purpose of this study is to investigate the performance of standard deconvolution and its ability to estimate reflection coefficient content directly from seismic data. We investigate three different ways to smooth the data spectrum to estimate the wavelet. We judge the quality of the wavelet estimation by comparing the estimated reflectivity to the know reflectivity in synthetic models. A synthetic zero-offset and shot gather data will be created and each of the deconvolution algorithms will be applied to them.

INTRODUCTION

Accurate acoustic impedance calculation is an important goal in seismic exploration. The most important information geophysicists have about the earth are recorded seismic data and these data are full of noises and very band limited. So the recorded data have only a small range of useful frequencies. Based on the convolutional model it is possible to estimate reflectivity via deconvolution algorithm (Oldenburg et. al., 1983). Deconvolution is a technique to estimate embedded wavelet which is then inverted and convolved with the data to calculate earth reflectivity. This technique can be done by various algorithms. Frequency domain spiking deconvolution (Margrave 2002), Wiener spiking deconvolution (Leinbach, 1995), Vibroseis deconvolution, Burg (maximum entropy) deconvolution (AuYeung, 1986) and Gabor deconvolution (Margrave & Lamoureux, 2002) are different types of deconvolution algorithms. Frequency domain spiking deconvolution which will be studied in this paper, smooths the spectrum of recorded data to estimate wavelet. The smoother can be frequency dependent or independent. Applied as a convolutional smoother, it can be any type of “bump” function like boxcar or Gaussian.

Here we will study about the performance of frequency domain deconvolution by changing the smoother type. Two types of synthetic data will be used in this study. A synthetic zero-offset seismogram created by *seismo* and a synthetic common shot gather created by *Syngram* both in the CREWES Matlab toolbox. To compare the results, the impedance inversion will be calculated by BLIMP (BandLimited IMPedance inversion, also in the CREWES toolbox).

METHOD

Perhaps the easiest deconvolution technique to conceptualize is the frequency domain method which is based on the convolutional model. Suppose a wave source can put energy into the ground, and the wave can propagate through the earth and be reflected by reflectors. Regardless of the effect of geometrical spreading, transmission losses, anelastic absorption and multiple reflections, a simple geophysical model can be introduced by a convolutional model. Mathematically, the seismic data recorded by a receiver are modelled as a convolution of earth's reflectivity function a known wavelet representing the source (Sheriff & Geldart, 1995).

$$s(t) = r(t) \bullet w(t), \quad (1)$$

where $s(t)$ is the recorded seismic data, $r(t)$ is the reflectivity function, $w(t)$ is the wavelet and “ \bullet ” is a convolutional operator. In the frequency domain, the convolutional operator changes to multiplication

$$s(f) = r(f)w(f). \quad (2)$$

In the real world, both earth reflectivity and wavelet are unknown and estimation of both functions are related to each other. It means that in equation 2 there are infinitely many possibilities for reflectivity and wavelet to give the same result in the left hand side. The frequency domain deconvolution method uses a simple concept. By assuming the reflectivity to have a white (or flat) amplitude spectrum, the amplitude spectral shape of the seismic trace is essentially similar to the spectral shape of the unknown wavelet (Figure 1). Thus all we need to do is smooth the amplitude spectrum of seismic trace to estimate amplitude spectrum of the deconvolution operator. Once the amplitude of deconvolution operator is calculated its phase can be calculated by the minimum phase assumptions as the Hilbert transform of the logarithm of the amplitude spectrum (Margrave, 2002). The complete reflectivity estimation process has been discussed in (Esmaili and Margrave, 2013).

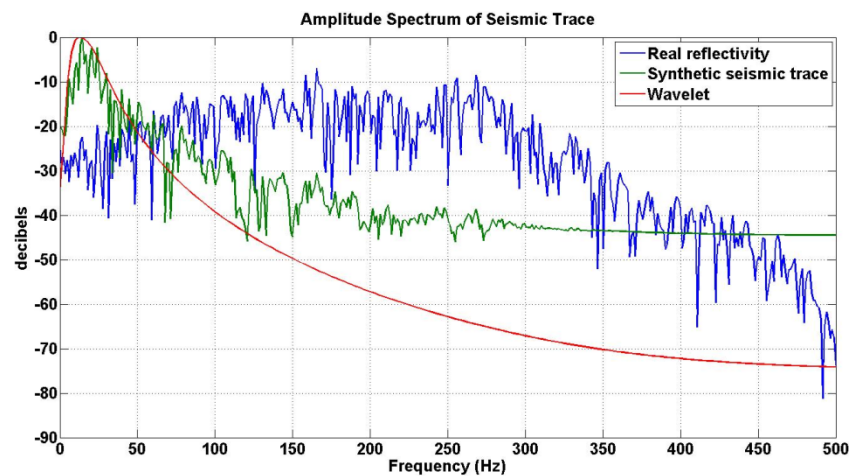


FIG.1. The amplitude spectral shape of seismic trace is similar to wavelet's one. Here the reflectivity is not actually which and this causes the wavelet to depart systematically from the smoothed shape of the trace spectrum

Transforming data from the time domain to the frequency domain by Fourier transform leads data to be expanded in negative and positive frequencies. However, the negative frequencies are often suppressed because they are redundant (that can be calculated for the positive frequencies). However, if we try to smooth the spectrum in only positive frequencies, the smoother gets significant errors at very low frequencies. Thus the power spectrum of data should be unwrapped first, then smoothed and then warped again for the inverse FFT.

Data smoothing can be done in different ways, including moving average, linear and seasonal exponential smoothing and Gaussian smoothing, etc. Since convolutional spectral smoothing becomes windowing in the time domain, it seems plausible that we might wish to have a convolutional frequency smoother whose width changes with frequency. In this study two different smoothers, boxcar and Gaussian, with constant and frequency dependent length will be examined.

Boxcar smoother

The simplest form of smoothing is the "moving average" which simply replaces each data value with the average of neighboring values. To avoid shifting the data, it is best to average the same number of values before and after where the average is being calculated. In equation form, the moving average is calculated by

$$\bar{x}[i] = \frac{1}{2M+1} \sum_{j=-M}^M x[i+j]. \quad (3)$$

Another term for this kind of smoothing is "boxcar smoothing". It can be implemented by convolving the input data with a box-shaped pulse with the length of n . The smoother with the length of n when applied to the input data, those points of data are located inside of smoother, are used to compute the average (figure 2).

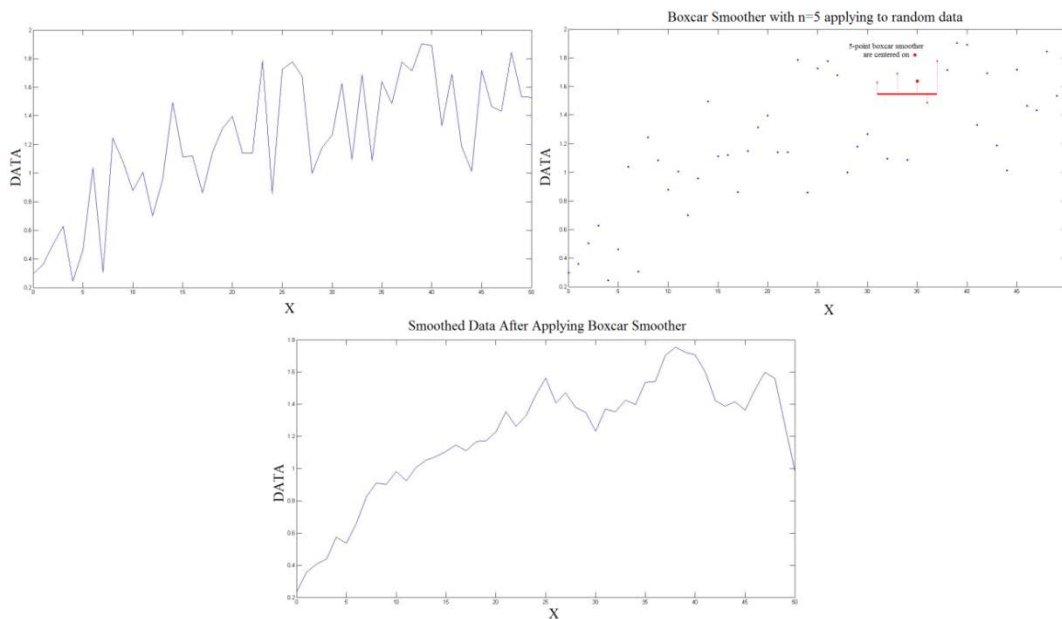


FIG.2. Boxcar smoothing procedure for the random data set.

Gaussian smoother

The Gaussian smoother is another type of convolutional smoother which is based on Gaussian distribution. In one dimension, the Gaussian function of zero mean is

$$G(x) = \frac{1}{\sqrt{2\pi\sigma^2}} e^{-\frac{x^2}{2\sigma^2}}, \tag{4}$$

where σ is the standard deviation of the distribution. Shown graphically, we see the familiar bell shaped Gaussian distribution (figure 3).

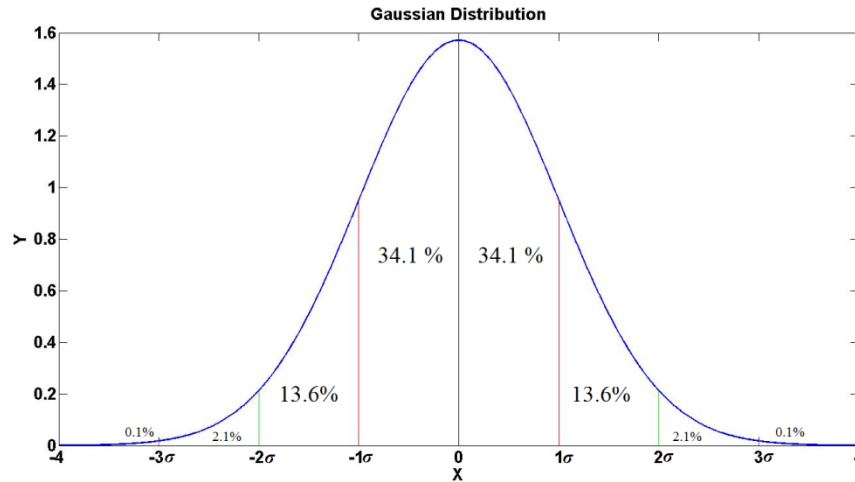


FIG.3. Gaussian distribution for using Gaussian smoother.

The standard deviation of the Gaussian function plays an important role in its behaviour. Figure 3 shows that the values located between $\pm \sigma$ account for 68% of the set, while 2σ from the mean account for 95% ($2 \times 13.6 + 2 \times 34.1$), and 3σ account for 99.7% so the distribution has approached very close to zero at about three standard deviations from the mean. This means we can normally limit the kernel size to contain only values within 3σ of the mean.

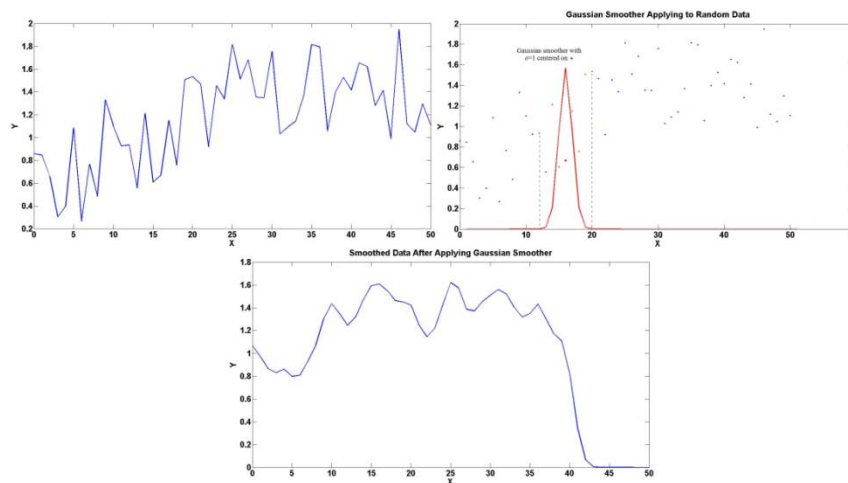


FIG.4. Gaussian smoothing procedure for the random data set.

In the figure 4 the Gaussian smoother with mean value of 15 and $\sigma=1$ is centered at the middle data point and it is applied to the indicated area. The same procedure is applied to every single point and the final smoothed data are shown in the last figure.

If the smoother length varies with frequency, we call it frequency-dependent Gaussian smoothing (FDGS).

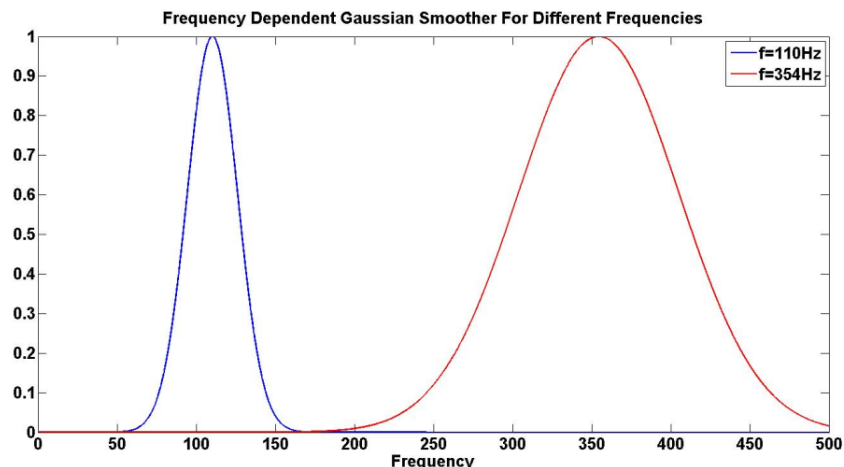


FIG.5. Schematic of changing Gaussian smoother length with frequency.

To investigate how these different smoothers can affect the deconvolution results, two different case studies will be discussed. A synthetic zero-offset single trace created by *seismo* and a synthetic AVO gather created with *Syngram* software both in CREWES Matlab toolbox. Both synthetic data will be created from well 12-27, located in Hussar, and 15Hz minimum phase wavelet with one millisecond sample rate.

ZERO-OFFSET DATA PROCESSING

First we start with synthetic zero-offset trace. These data are created with *seismo* in CREWES toolbox. Based on equation 1, *seismo* is taking the reflectivity from well log and convolving it with the wavelet to create a synthetic seismic trace. The synthetic seismogram and well reflectivity are shown in figure 6.

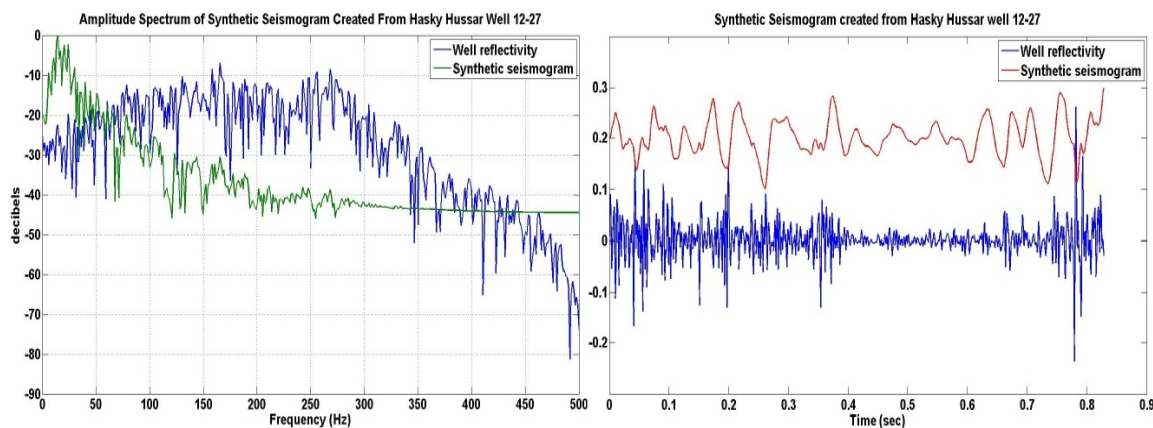


FIG.6. Zero-offset synthetic data in time domain and its amplitude spectrum in frequency domain.

Deconvolution algorithm with boxcar smoother (BS)

The first choice of deconvolution operator uses the boxcar smoother. As mentioned before the number of points of boxcar function is our smoother length. First we need to choose the best smoother length for each trace. To do this, a series of tests were conducted in which the smoother length was varied over a reasonable range and the resulting reflectivity estimates were crosscorrelated with the known reflectivity. The results, plotted in Figure 7 shows the best length of smoother in frequency for the zero-offset synthetic seismic trace to be about 4.8Hz. 4.8Hz. Since the length of the synthetic in Figure 6 about $T = 0.85$ s, the smoother width in Hz is related to the number of points in the smoother by

$$f_{smooth} = n_{smooth} \Delta f = \frac{n_{smooth}}{T}, \tag{5}$$

where f_{smooth} and n_{smooth} are length of smoother in frequency and smoother length in point number respectively.

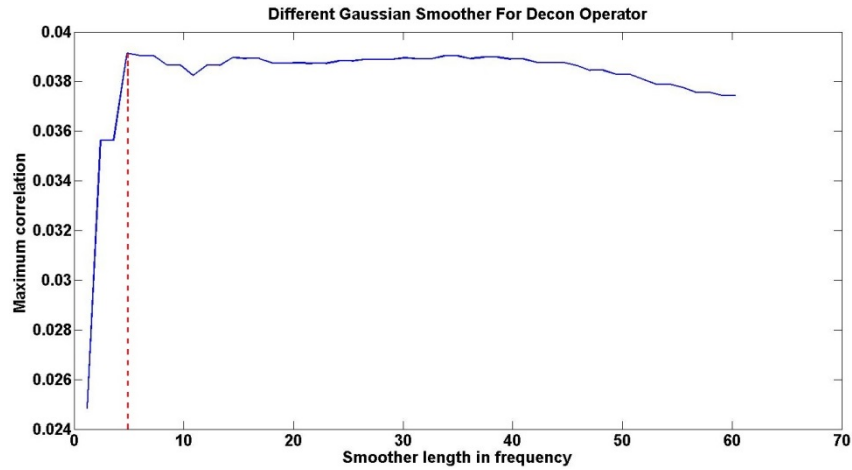


FIG.7. Finding the best choice for the boxcar smoother length in frequency.

According to this figure 4.8Hz (4 samples) is the optimum smoother length can be chosen for the deconvolution operator based on boxcar smoother. The result of boxcar-smoothing with length of 4.8Hz, frequency-domain deconvolution is shown in figure 8.

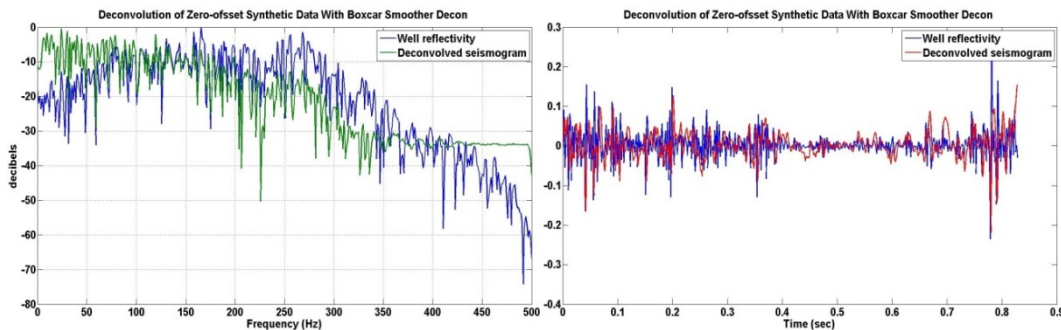


FIG.8. Deconvolution of zero-offset synthetic seismic trace with boxcar smoother decon at frequency domain and time domain.

Deconvolution algorithm with constant Gaussian smoother (CGS)

The next possible option of smoother to smooth the amplitude spectrum of data in deconvolution operator is constant Gaussian smoother. As mentioned before, the Gaussian smoother is defined by equation 4 and its length indicated by σ . σ is half width of Gaussian distribution which the value of Gaussian reaches to $e^{-1/2}$ of its maximum. The mathematical equation of Gaussian smoother we are using in this study is

$$\bar{A}_j = \frac{\sum_k A_k g_{j-k}}{\sum_k g_k}, \quad (6)$$

where A_k is the unsmoothed amplitude spectrum, \bar{A}_j is the smoothed spectrum, and

$$g_k = e^{-(k\Delta f)^2 / \sigma_f^2} \quad (7)$$

in which σ_f is the standard deviation in Hz.

Here σ_f is the length of smoother in frequency. Again it is possible to choose the best length of smoother for each trace. The curve of maximum correlation between deconvolved trace and reflectivity and length of smoother is illustrated in figure 9. According to the figure 9 the maximum correlation will achieved if the length of smoother is 49Hz .

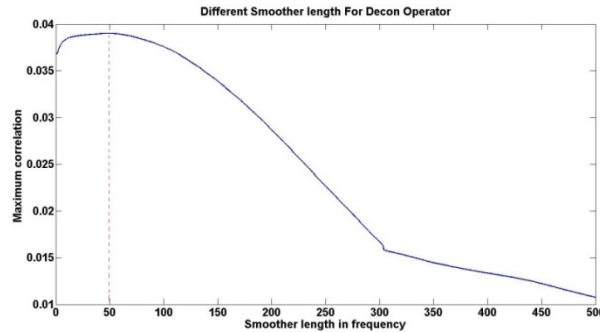


FIG.9. Finding the best choice for the constant Gaussian smoother length in frequency.

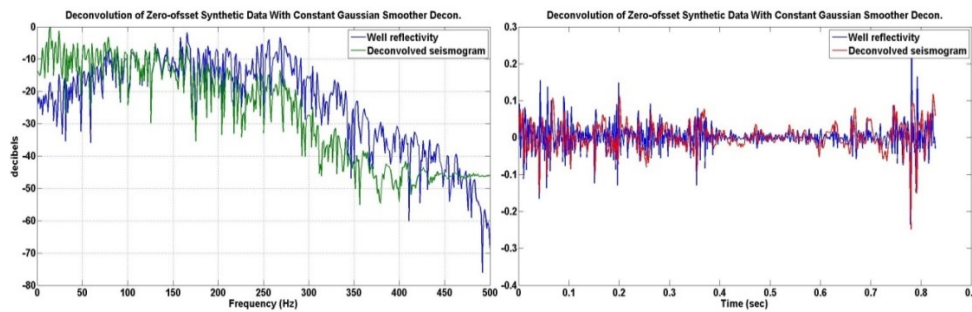


FIG.10. Deconvolution of zero-offset synthetic seismic trace with constant Gaussian smoother decon at frequency domain and time domain.

Decon algorithm with frequency dependent Gaussian smoother (FDGS)

As previously mentioned, the idea of changing smoother length with frequency comes from the consideration that spectral smoothing must be time-domain windowing and lower frequencies should require longer temporal windows. This implies that the frequency domain smoother should decrease as frequency tends towards zero. So we will define a smoother length which becomes short in low frequencies and long in high frequencies. We do this in a similar fashion to equation 7 except that we set σ_f to depend on frequency according to

$$\sigma_f = \frac{f}{n} = \frac{k\Delta f}{n}, \tag{8}$$

where n is a deconvolution input parameter and indicates the rate of variation of smoother length and its best value can be find similarly to the two previous methods. Figure 11 shows the maximum correlation between first trace and reflectivity versus n .

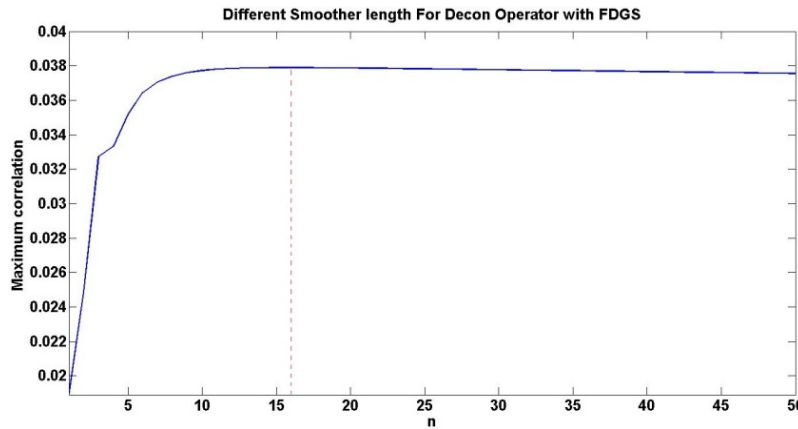


FIG.11. Finding the optimum value for n in frequency dependent Gaussian smoother length.

The best value for n is 16. So the smoother length can be varied by $\frac{f}{16}$. For instance the Gaussian distribution is shown for 50Hz and 250 Hz in figure 12.

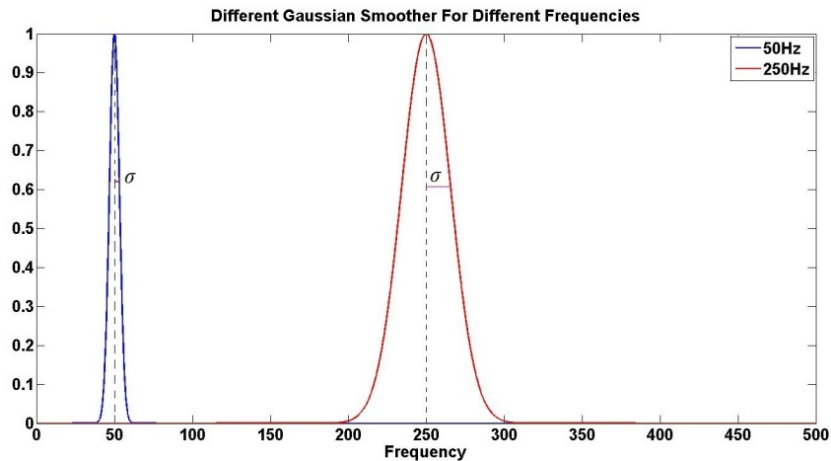


FIG.12. Different Gaussian smoother for various frequencies.

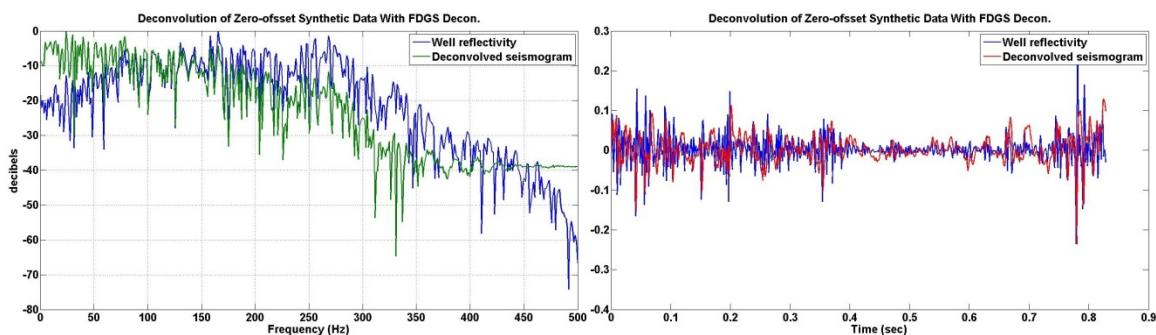


FIG.13. Deconvolution of zero-offset synthetic seismic trace with FDGS decon at frequency domain and time domain.

As we can see in frequency domain plots in figures 8, 10 and 13 there are huge differences between amplitude spectrum of real reflectivity and estimated reflectivity in frequencies below than 75Hz. These big differences are the result of white spectrum assumption of deconvolution algorithm (Margrave 2002) and it can be fixed by a colour operator (Esmaeili and Margrave, 2014). The comparison of these three deconvolution algorithms results will be discussed in the last section.

SYNTHETIC AVO GATHER PROCESSING

The next case study in this paper is about synthetic data with non-zero offsets. For this case the synthetic data are created by *Syngram* software in CREWES Matlab toolbox. The source is located at the origin and 21 receivers are located in every 50 meters starting from origin and ending at 1000 meters. *Syngram* is that it assumes the same vertical velocity model for whole studied area (figure 14).

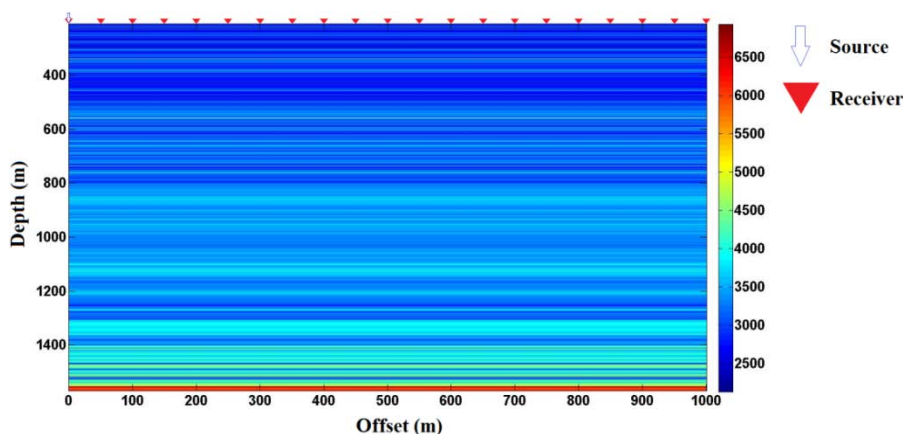


FIG.14. Schematic of source and receivers location for the seismic model.

Figure 15 shows the noise free synthetic AVO gather created from well 12-27 log and 15Hz minimum phase wavelet. The normal moveout effect is clear and the top parts of far offset traces are muted because of removing critical angle effect.

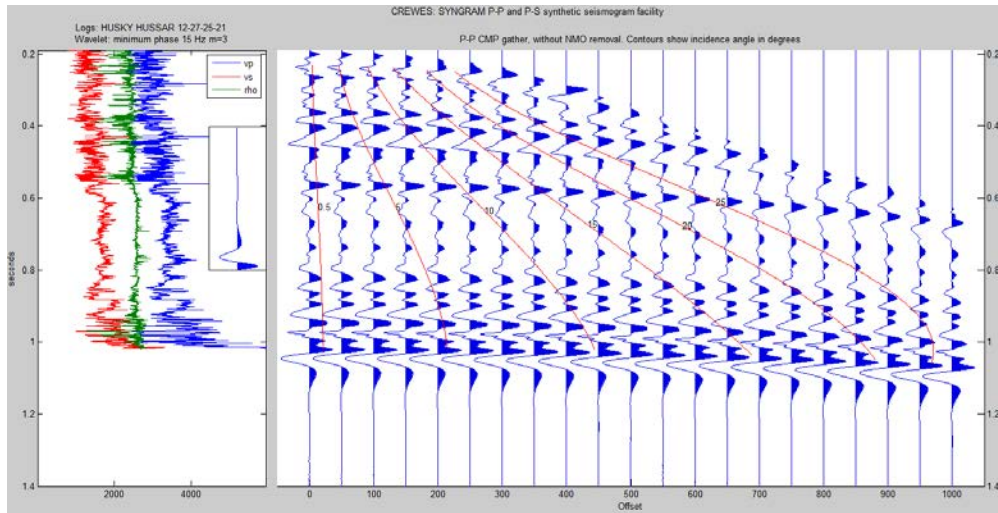


FIG.15. Synthetic common shot gather created by syngram.

The deconvolution algorithm should be applied for each trace with appropriately defined design window. We define a design window for whole the gather as shown in Figure 16 that includes the same reflectivity zone on each trace. The boundaries are defined by RMS velocity and starts from $t=0.6$ sec and ends in 1sec in the first trace.

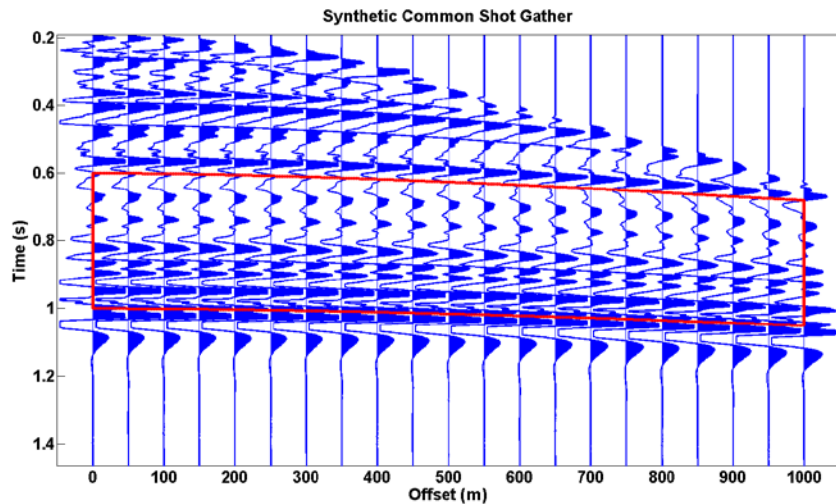


FIG.16. Synthetic shot gather and the appropriate design window.

Deconvolution algorithm with boxcar smoother (BS)

Like the zero-offset data, we start with boxcar smoother for deconvolution algorithm. The input parameter of boxcar smoother deconvolution algorithm for smoother length is a point number, n_{smooth} in equation 5, and should be converted to smoother length in frequency. Finding the best value for smoother length with comparing maximum correlation between well reflectivity and deconvolved trace is possible. For the first trace it is illustrated in the figure 17.

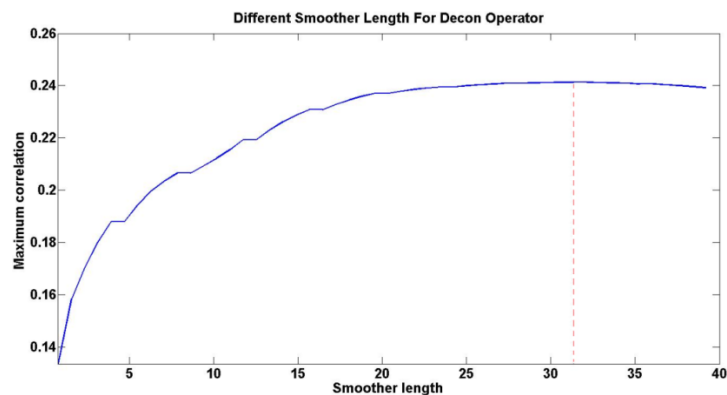


FIG.17. Finding the best choice for the boxcar smoother length in frequency.

According to this figure the best option for the length of boxcar smoother is 31.34Hz. Once the smoother length is calculated for each trace the deconvolution operator can be applied to them. Figure 18 shows the deconvolved AVO gather traces.

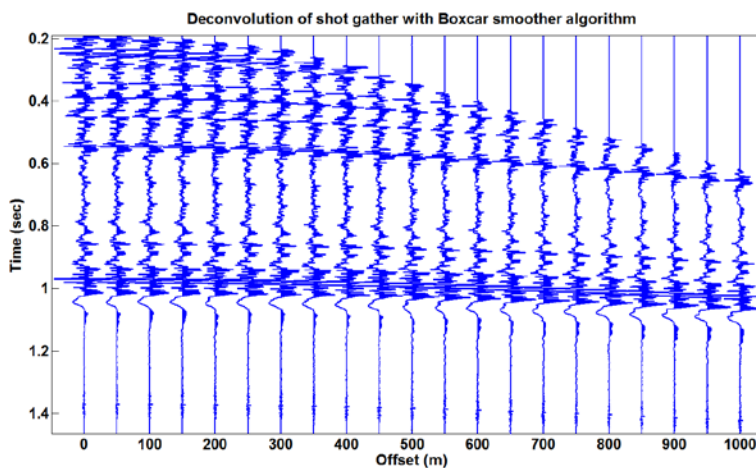


FIG.18. Deconvolution of shot gather with boxcar smoother deconvolution.

Now we need to remove the normal move out from deconvolved data based on RMS velocity. The reflectivity estimation at zero offset can be estimated by stacking the NMO removed traces. The NMO-removed data are illustrated in the next figure.

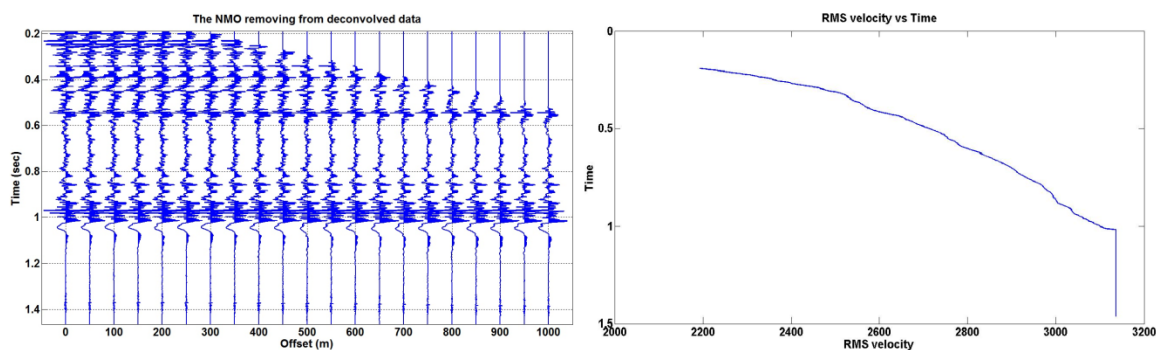


FIG.19. Deconvolved trace after removing NMO (left) and RMS velocity (right).

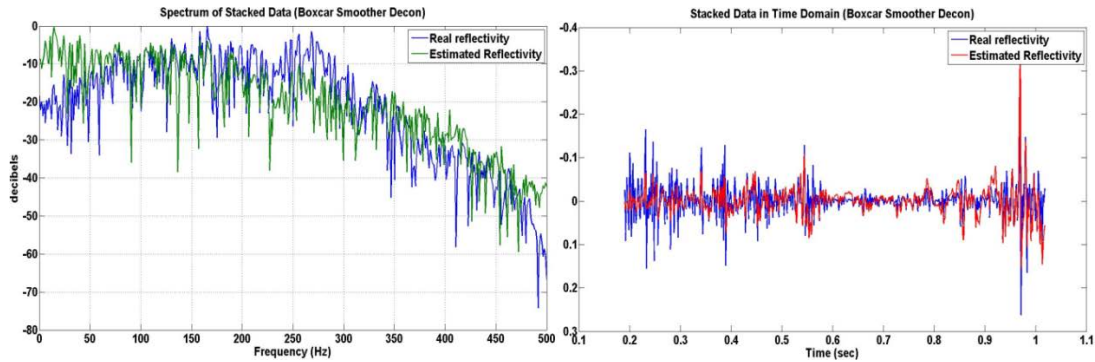


FIG.20. Comparing stacked data and real reflectivity on both frequency and time domain resulted from Boxcar smoother decon algorithm.

Deconvolution algorithm with constant Gaussian smoother (CGS)

Like the deconvolution of zero-offset data with constant Gaussian smoother, we are using the same smoother for every single trace of shot gather (equation 6). Again the length of smoother is very important and needs to be determined. We are using the same technique to find the optimum smoother length for deconvolution of every trace of shot gather. For example for the first trace the smoother length become 61Hz (figure 21).

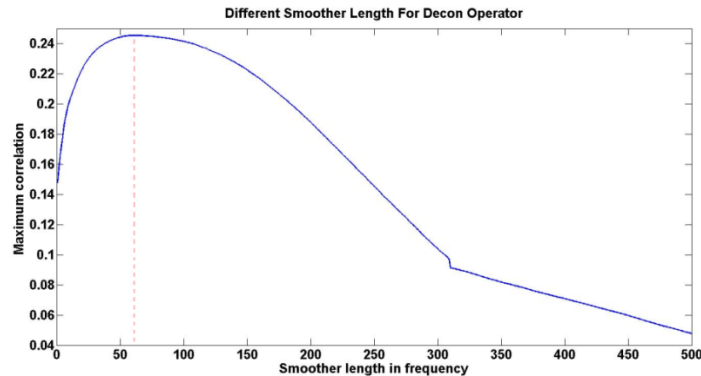


FIG.21. Finding the best choice for the Gaussian smoother's length in frequency.

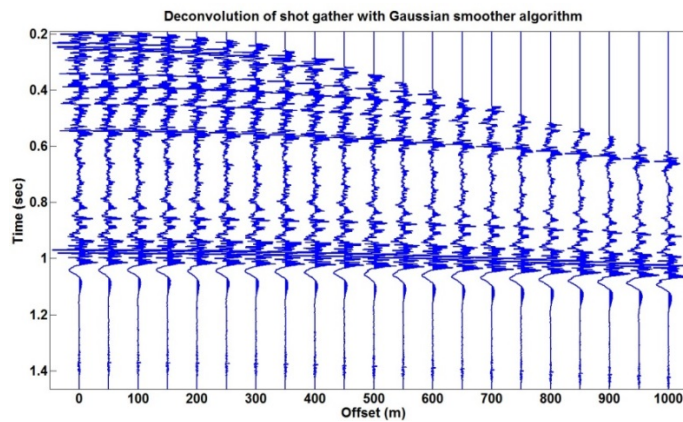


FIG.22. Deconvolution of shot gather with constant Gaussian smoother algorithm.

The NMO removed data are illustrated in figure 23.

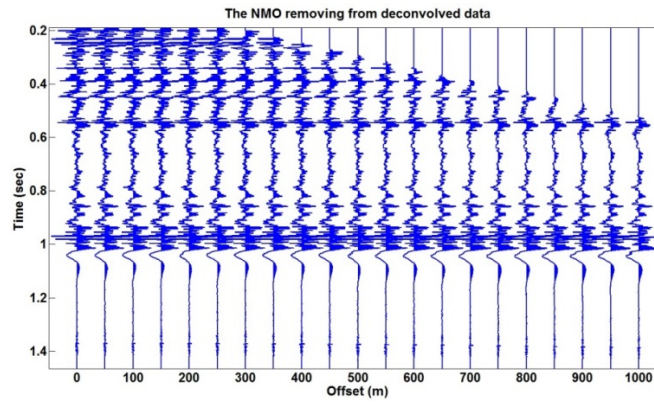


FIG.23. deconvolved trace by constant Gaussian smoother decon after removing NMO.

And finally stacking all these traces gives us the estimated reflectivity at zero offset. Figure 24 shows the result of stacked data in both time and frequency domain.

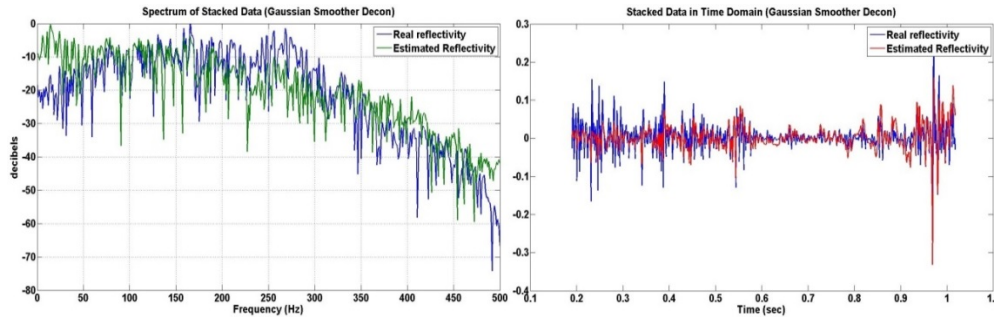


FIG.24. Comparing stacked data and real reflectivity on both frequency and time domain resulted from Gaussian smoother decon algorithm.

Decon algorithm with frequency dependent Gaussian smoother (FDGS)

As explained previously for deconvolution of zero-offset data with FDGS algorithm, the input parameter for indicating smoother length was n , which is the rate of length variation in terms of frequency. Once the n is computed the frequency dependent smoother length can be calculated by equation 8.

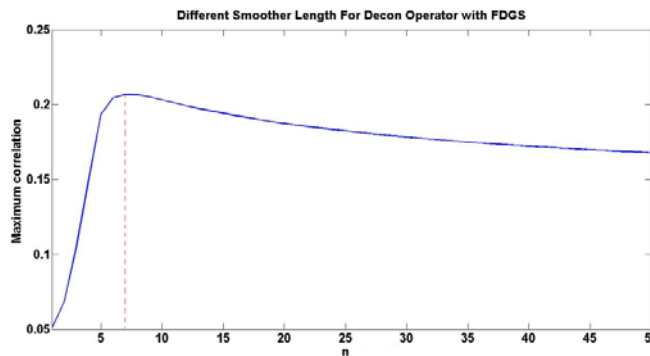


FIG.25. Finding the best choice for the frequency dependent Gaussian smoother's length.

Figure 25 shows that the best frequency variation rate for smoother's length is $n=7$. Using this technique and applying it to the all traces gives us the deconvolved trace in time domain. Again the normal moveout should be removed right after that and then the data are ready to be stacked. Figures 26 and 27 show these procedures.

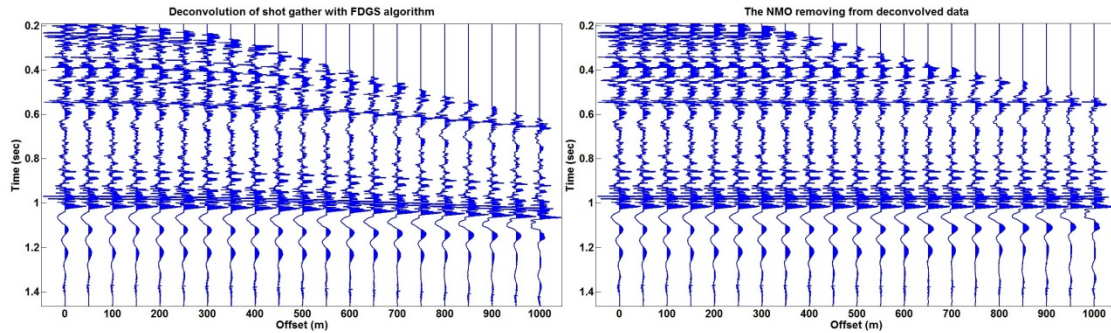


FIG.26. Deconvolved shot gather with FDGS algorithm (left) and removing NMO from deconvolved data (right)

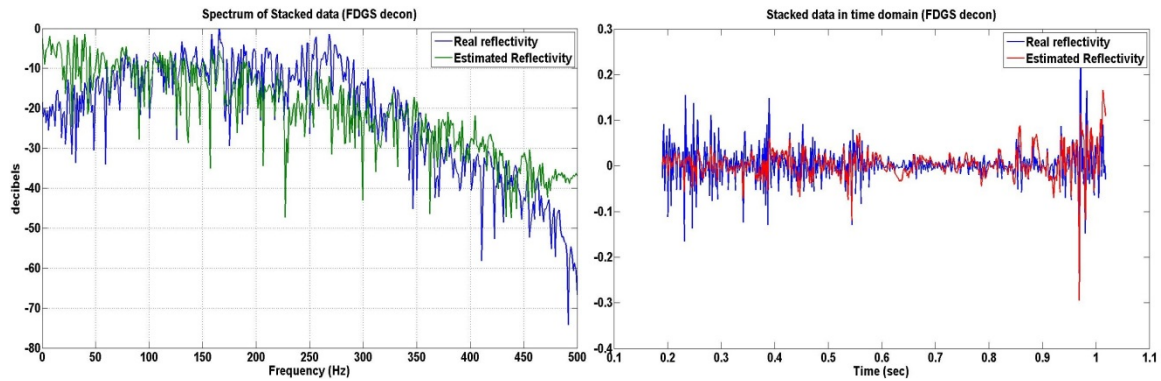


FIG.27. Comparing stacked data and real reflectivity on both frequency and time domain resulted from FDGS decon algorithm.

ERROR ESTIMATION BY IMPEDANCE INVERSION

The final goal of reflectivity estimation is computing earth acoustic impedance. Trying to estimate the reflectivity from bandlimited seismic data as it was illustrated in the last section is so challenging. The acoustic impedance, which is the multiplication of velocity and density, is related to reflectivity and can be calculated by (Esmaeili and Margrave, 2013)

$$I_{n+1} = I_1 \prod_{j=1}^n (e^{2r_j}) = I_1 e^{2 \sum_{j=1}^n r_j} \quad (9)$$

where r_j is the reflectivity and I_{n+1} is acoustic impedance. Any misestimation of reflectivity will directly affect the estimation of acoustic impedance. Incorrect low frequency reflectivity causes an incorrect trend of impedance and incorrect high frequency reflectivity causes poor detail in the impedance. For example figure 28 shows

the impedance computed directly from equation 9. The reflectivity is assumed be the result of zero-offset data deconvolution with boxcar smoother.

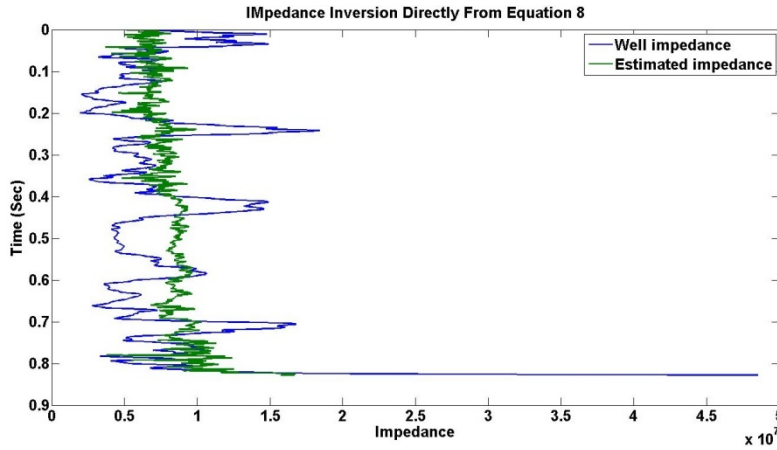


FIG.28. The effect of wrong reflectivity estimation on impedance inversion.

Ferguson and Margrave (1996) created the BLIMP (BandLimited IMPedance) algorithm which is available in CREWES Matlab toolbox to input the low frequencies data from well log data. There is low and high cut-off frequency in this algorithm which is filtering the signal out of this area and then the algorithm import the data from log for the cut-off area.

The impedance inversion for the results of three different smoother for both zero-offset data and shot gather data are shown in figure 29 and 30. The BLIMP algorithm has been used for all cases.

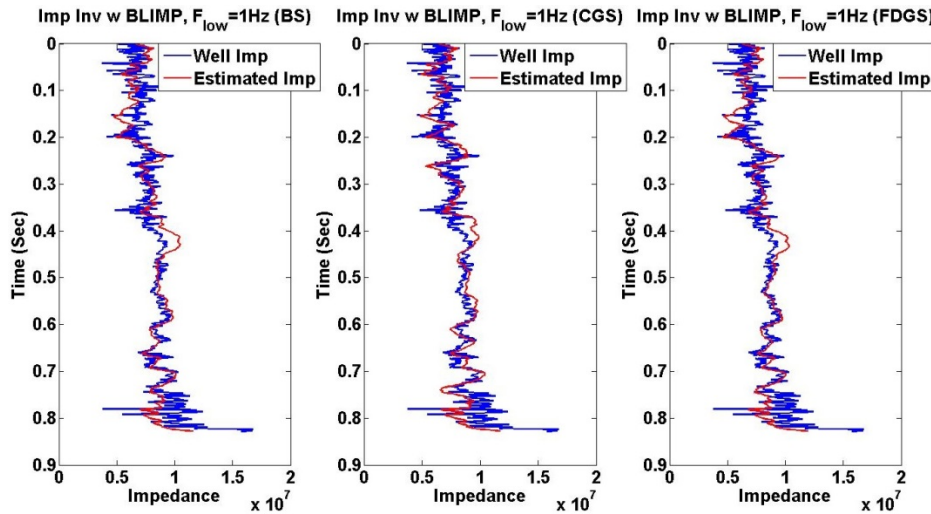


FIG.29. Impedance inversion using BLIMP algorithm with low cut-off frequency of 1Hz for three reflectivities resulted from three different deconvolution algorithms (zero-offset data).

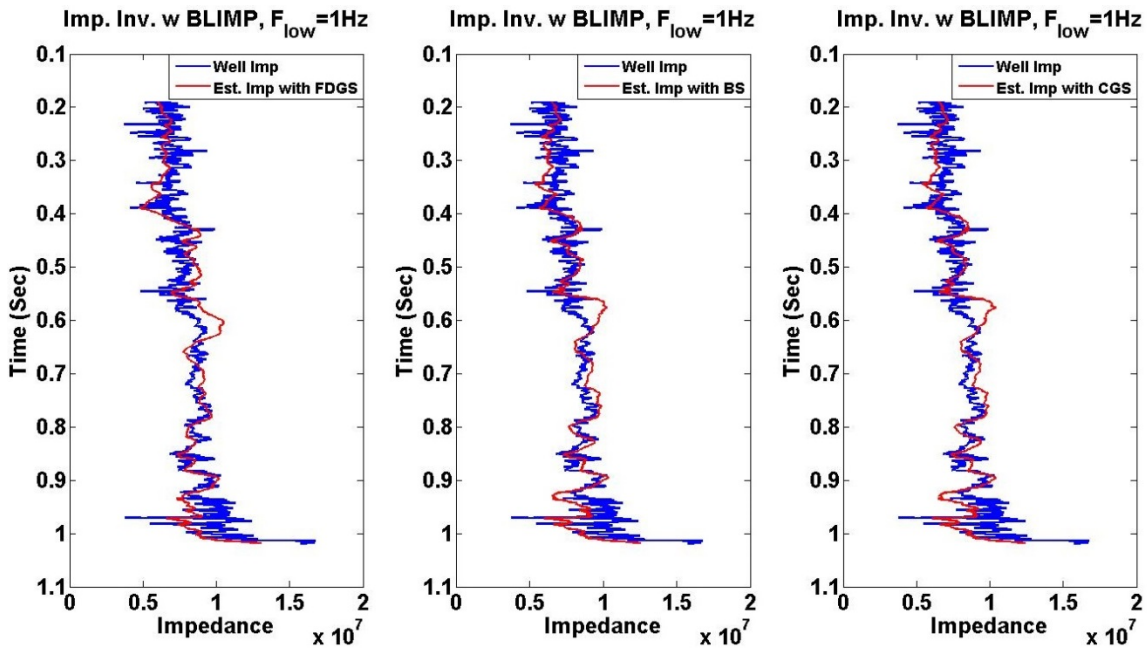


FIG.29. Impedance inversion using BLIMP algorithm with low cut-off frequency of 1Hz for three reflectivities resulted from three different deconvolution algorithms (common shot gather data).

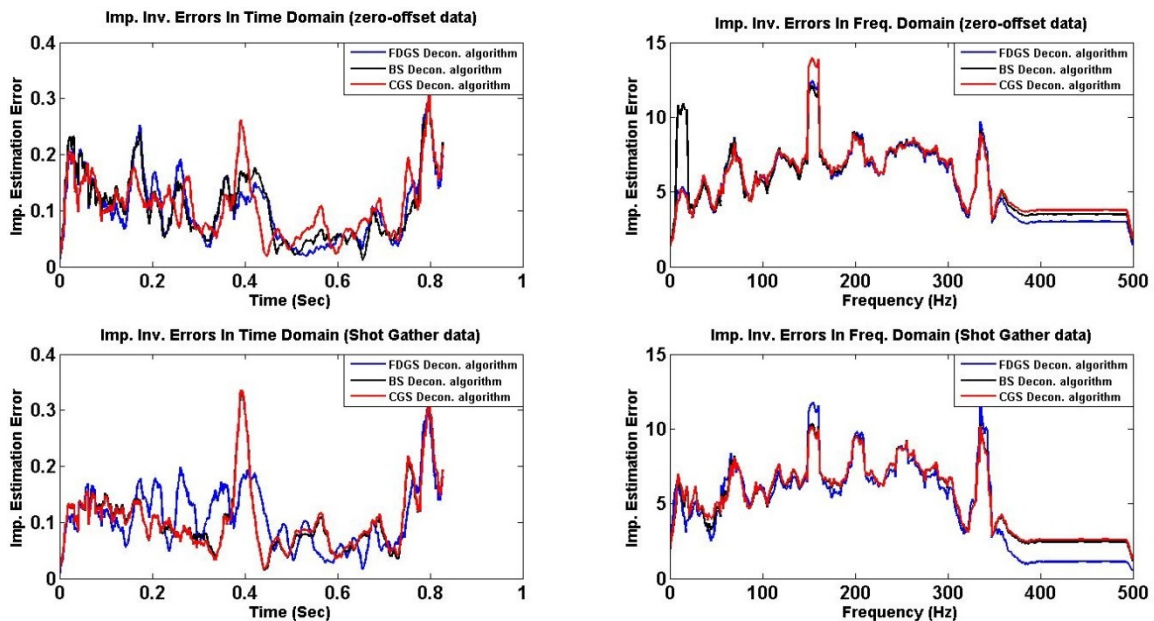


FIG.30. Impedance estimation errors from zero-offset data (left) and common shot gather data (right) with three different deconvolution algorithms.

From the figure 30, which shows the error between well impedance and estimated impedance for synthetic zero-offset and shot gather data, it is hard to say which one of our deconvolution algorithms work better related to the other ones. It is also hard to say how much the different smoother could affect the low frequency components. From correlation point of view, the maximum correlation between estimated impedance from zero-offset data and well impedance for FDGS, CGS and BS are respectively 0.9898,

0.9897 and 0.9896. Also the maximum correlation between impedance inversion and synthetic shot gather data for three mentioned deconvolution algorithms are 0.9898, 0.9896 and 0.9896.

On the other hand, from figures 8, 10, 13, 20, 24 and 27 in frequency domain it is clear that even by choosing the best smoother for deconvolution algorithm, there are many differences in low frequencies. Esmaeili and Margrave (2014) modeled a color operator to apply to the deconvolved trace for correcting low frequency components (figure 31). Their results show that applying color operator to the deconvolved trace right after deconvolution can correct most of low frequency components.

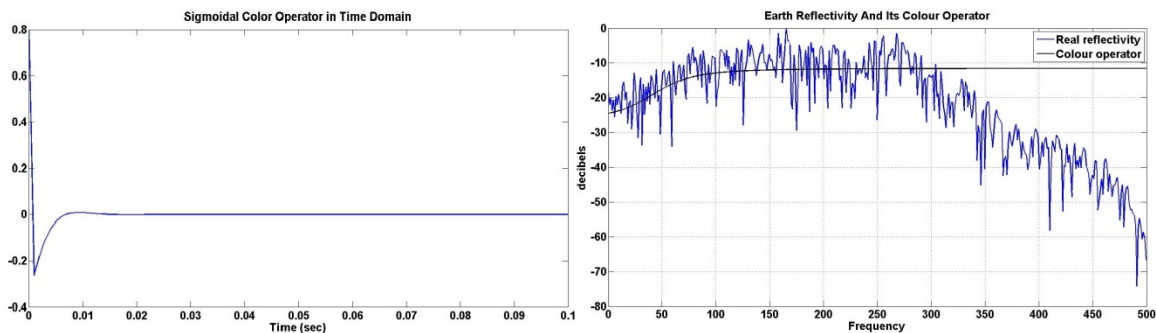


FIG.31. Amplitude spectrum of well Husky 12-27 reflectivity and its Sigmoidal color operator.

This color operator into the deconvolved traces of synthetic zero-offset and shot gather data with three different smoother has been applied and their results in frequency domain are shown in figure 32 and 33.

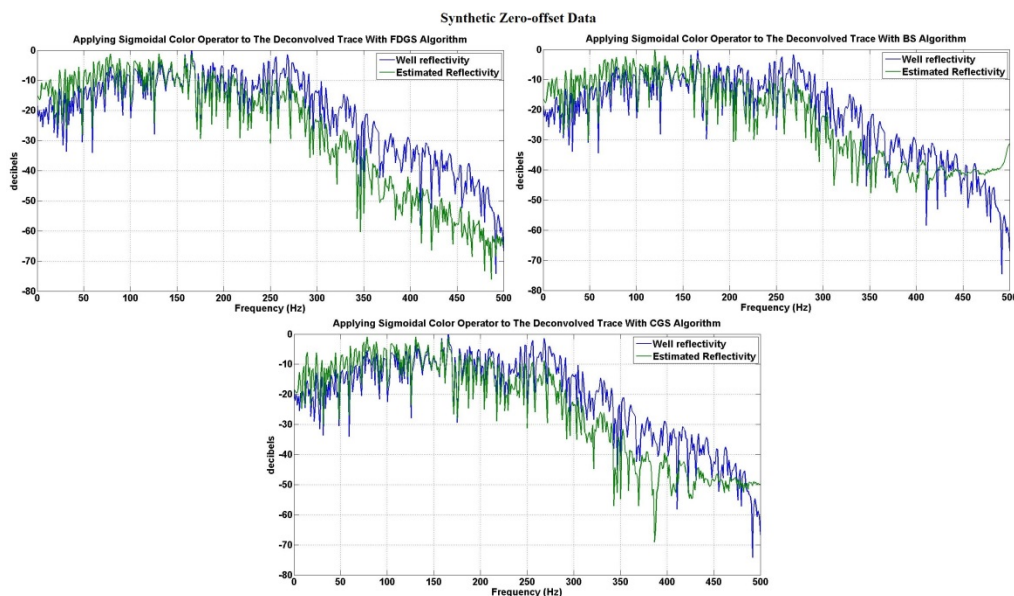


FIG.32. Applying Sigmoidal color operator to synthetic zero-offset data results from three different deconvolution algorithms.

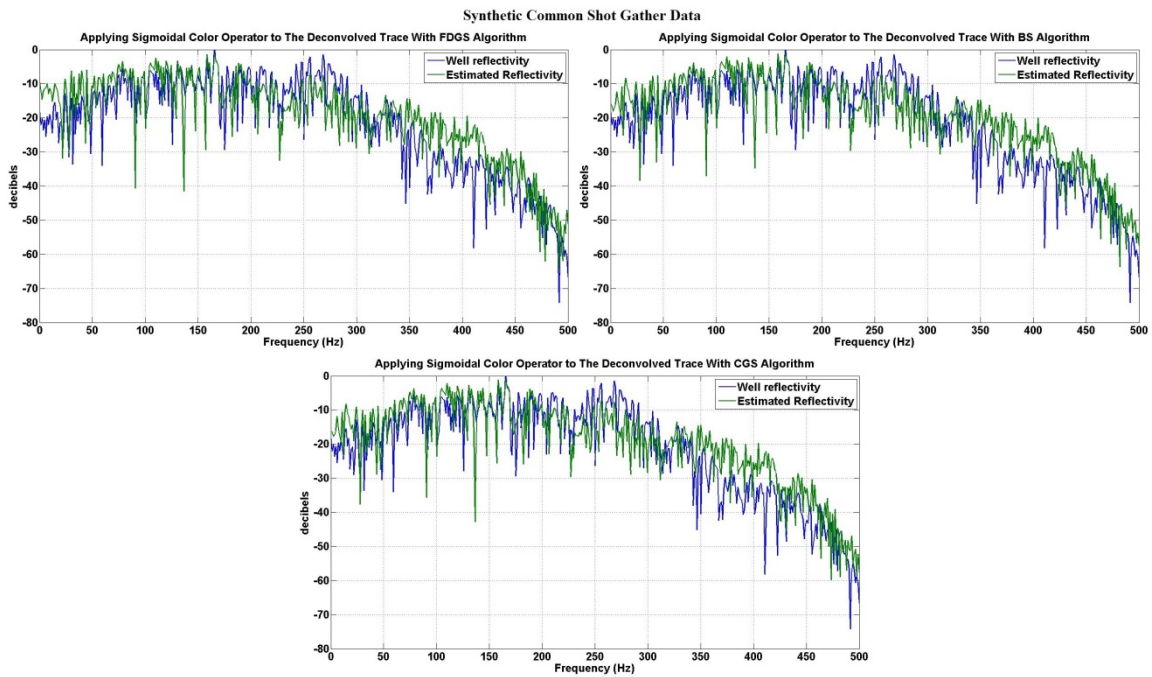


FIG.33. Estimated Reflectivity after applying color operator to the deconvolved shot gather data with three different deconvolution algorithms.

As it is clear from these figures the amplitude spectrum of estimated data resulted from both zero-offset and shot gather data, after applying color operator to their deconvolved trace, can be improved significantly. It is also possible to compute the acoustic impedance using BLIMP algorithm with 1Hz low cut-off frequency to see the results in low frequencies.

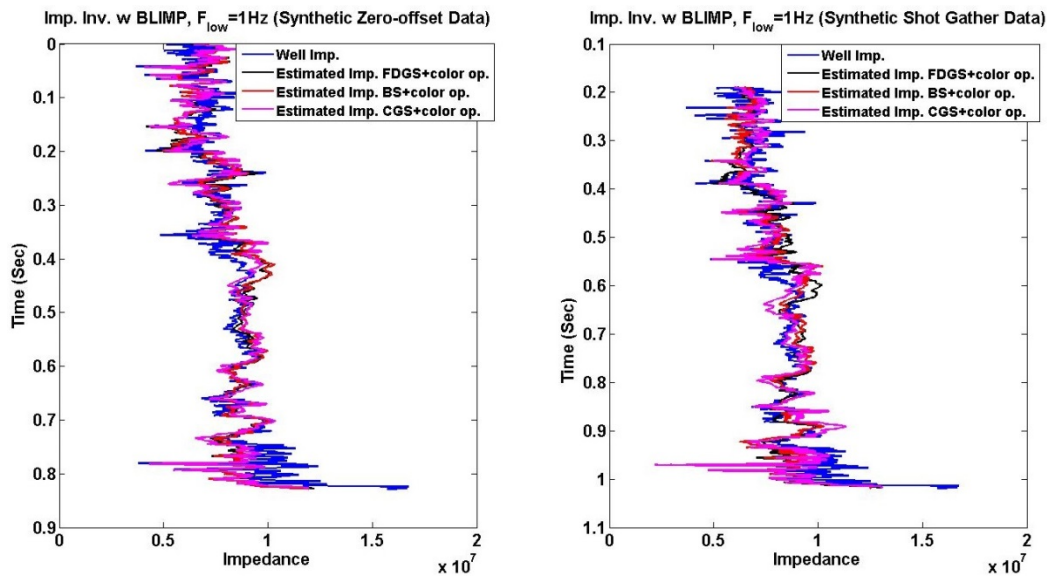


FIG.34. Impedance inversion results after applying color operator to the synthetic zero-offset (left) and synthetic shot gather (right) data with BLIMP algorithm.

Synthetic Zero-offset Data

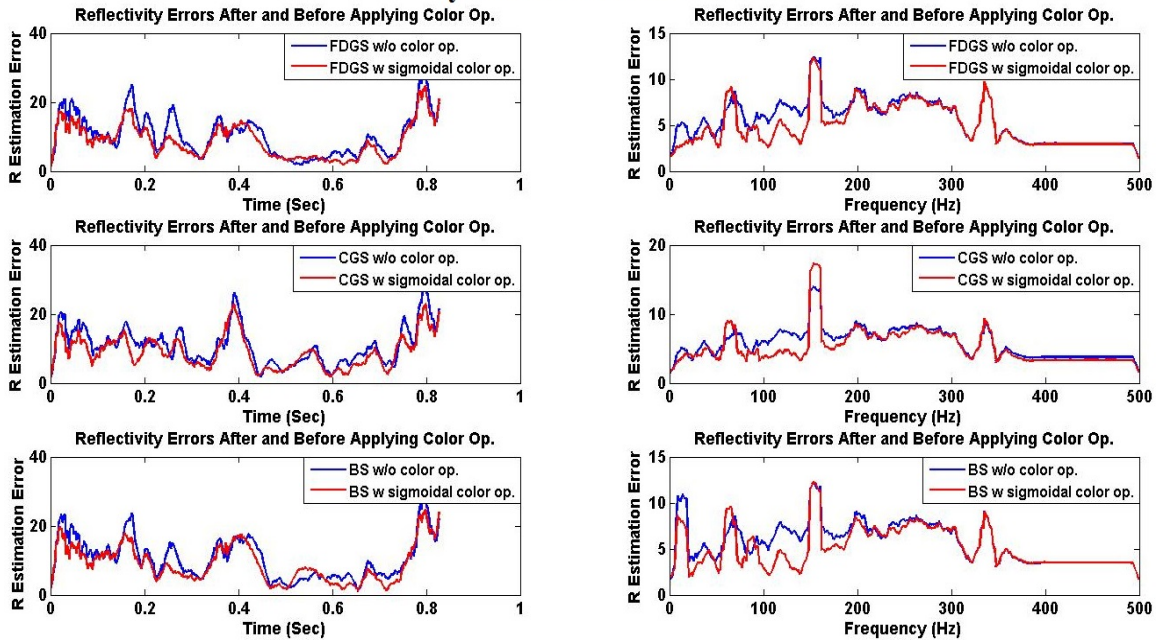


FIG.35. Impedance estimation errors for synthetic zero-offset data before and after applying color operator to each of deconvolution algorithm.

Synthetic Shot Gather Data

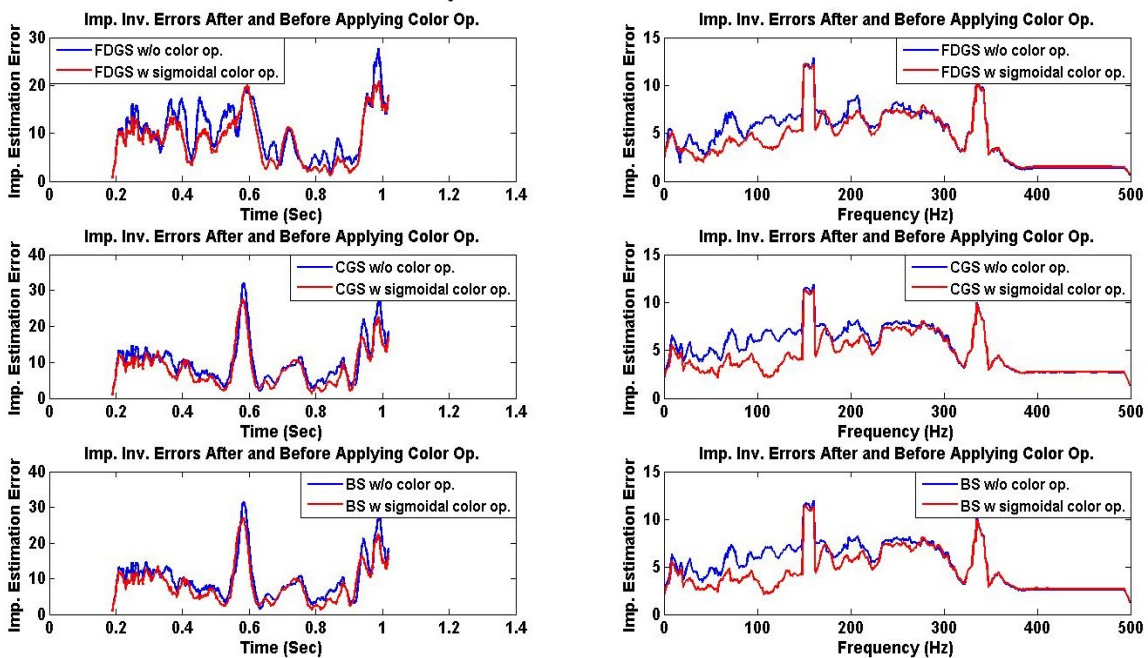


FIG.36. Impedance estimation errors for synthetic shot gather data before and after applying color operator to each of deconvolution algorithm.

CONCLUSION

Choosing the different smoothers can affect the reflectivity estimation. However in the low frequencies trying to estimate the reflectivity is not affected significantly with changing smoother. Though, by applying color operator to any deconvolved data resulted from either synthetic zero-offset or shot gather data, it is possible to improve the impedance inversion significantly in frequencies around higher than 8Hz. The results also suggest that the Constant Gaussian smoother (CGS) and Frequency Dependent Gaussian Smoother (FDGS) if they have been chosen as deconvolution smoother, their results become improved after applying color operator.

ACKNOWLEDGEMENTS

We thank the sponsors of CREWES for their supporting and gratefully acknowledge support from NSERC (Natural Science and Engineering Research Council of Canada) through the grant CRDPJ 379744-08. And also we would like to thank all the students and staff in CREWES.

REFERENCES

- AuYeung, C. (1986). Maximum entropy deconvolution. *IEEE International Conference on ICASSP '86. (Volume:11)*, (pp. 273 - 276).
- Esmaeili, S., & Margrave, G. F. (2013). Recovering low frequencies for impedance inversion by frequency domain deconvolution. *CREWES research report, Vol. 25*.
- Ferguson, R. J., & Margrave, G. F. (1996). A simple algorithm for bandlimited impedance inversion. *CREWES research report, Vol. 8, No. 21*.
- Leinbach, J. (1995). Wiener spiking deconvolution and minimum-phase wavelets: A tutorial. *Geophysics*.
- Margrave, G. F. (2002). *Methods of seismic data processing*. Calgary: Department of Geoscience, University of Calgary.
- Margrave, G. F., & Lamoureux, M. P. (2002). Gabor deconvolution. *CSEG Geophysics*.
- Oldenburg, D. W., Scheuer, T., & Levy, S. (1983). Recovery of the acoustic impedance from reflection seismograms. *Geophysics*, 1318-1337.
- Sheriff, R. E., & Geldart, L. P. (1995). *Exploration Seismology*. Cambridge University Press.